

Supplementary material: Characterisation of precipitates in Mg-Sn alloys

Peak-aged Mg-6Sn alloy

Two types of Mg_2Sn precipitate were found in the peak aged Mg-6Sn binary alloy. STEM-HAADF images showing the microstructure of the peak aged Mg-6Sn are shown below in Figure 1. The basal laths with long axis along the $\langle 11\bar{2}0 \rangle_{\text{Mg}}$ directions are named Type 1 precipitates while the basal laths with long axis along the $\langle 10\bar{1}0 \rangle_{\text{Mg}}$ directions are named Type 2 precipitates. Both precipitate types are marked with arrows. The peak aged binary alloy is dominated by lath-shaped precipitates with a habit plane of $(0001)_{\text{Mg}}$ (basal plane).

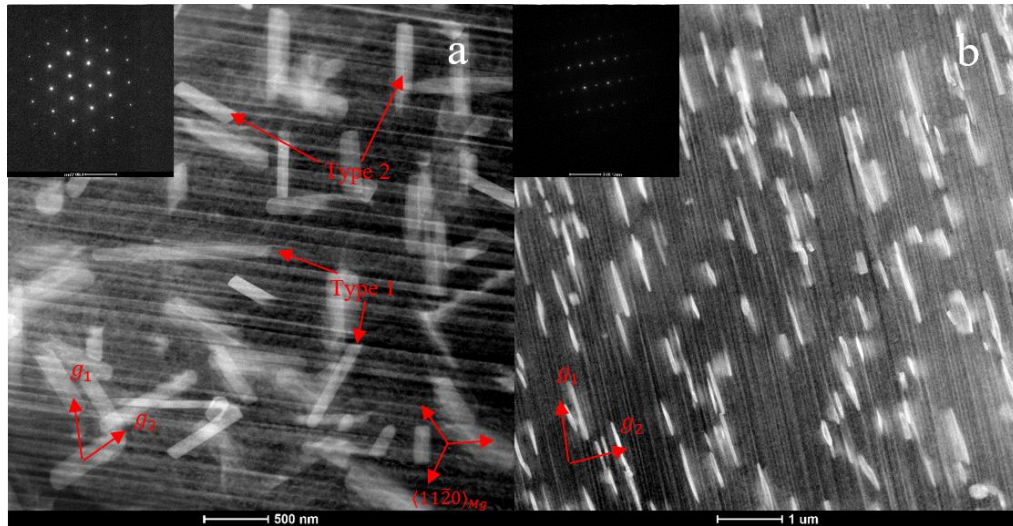


Figure 1 STEM-HAADF image showing the general microstructure of the peak aged Mg-6Sn binary alloy, (a) $B \approx [0001]_{\text{Mg}}$, $g_1 = 10\bar{1}0_{\text{Mg}}$, $g_2 = 01\bar{1}0_{\text{Mg}}$, (b) $B \approx [11\bar{2}0]_{\text{Mg}}$, $g_1 = 10\bar{1}0_{\text{Mg}}$, $g_2 = 0002_{\text{Mg}}$

A STEM-HAADF image showing the exact morphology of a Type 1 precipitate can be found in Figure 2. Type 1 laths tend to have round tips and an aspect ratio normally around 10:1. A selected area diffraction pattern indicating the OR between the Type 1 precipitates and the Mg matrix is shown in

Figure 3. As can be seen from the diffraction pattern, the OR between the Mg-matrix and the Type 1 precipitates is $(0001)_{\text{Mg}} \parallel (110)_{\text{Mg}_2\text{Sn}}$, $[11\bar{2}0]_{\text{Mg}} \parallel [001]_{\text{Mg}_2\text{Sn}}$. This OR is equivalent to the OR1 first reported by Henes & Gerold and also in some other studies[1]–[3].

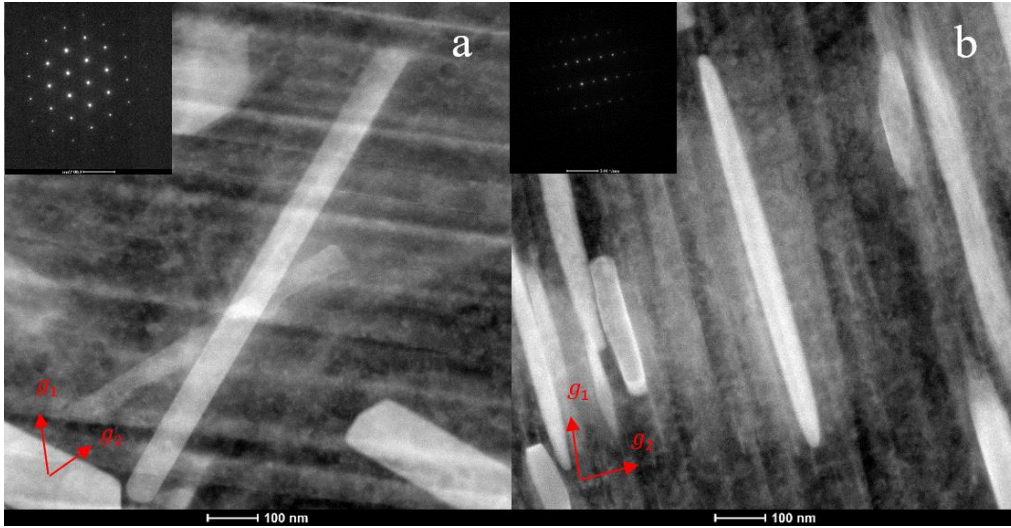


Figure 2 STEM-HAADF image showing the morphology of a Type 1 basal lath, (a) $B \approx [0001]_{Mg}$, $g_1 = 10\bar{1}0_{Mg}$, $g_2 = 01\bar{1}0_{Mg}$, (b) $B \approx [11\bar{2}0]_{Mg}$, $g_1 = 1\bar{1}00_{Mg}$, $g_2 = 0002_{Mg}$

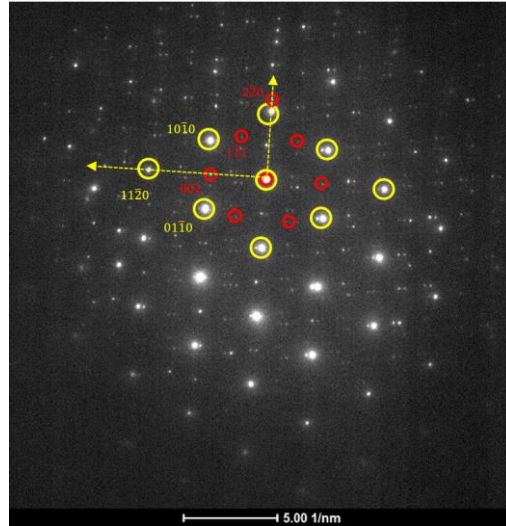


Figure 3 Selected area diffraction pattern determining the OR between a Type 1 precipitate and the Mg matrix. Reflections from the $[0001]_{Mg}$ zone axis are marked with yellow circles; reflections from the $[110]_{Mg2Sn}$ zone axis are marked with red circles. The OR given by the diffraction pattern is $(0001)_{Mg} \parallel (110)_{Mg2Sn}$, $[11\bar{2}0]_{Mg} \parallel [001]_{Mg2Sn}$.

The morphology of the Type 2 precipitates is shown in a STEM-HAADF image in Figure 4. Compared with the Type 1 precipitates, the Type 2 precipitates tend to have a smaller aspect ratio, around 5:1. In addition, differently from the round tips of the Type 1 precipitates, Type 2 precipitates exhibit three obvious facets which are marked by arrows in Figure 4(a). One of the facets is parallel to $\{11\bar{2}0\}_{Mg}$ (F1) while the other two facets are parallel to $\{10\bar{1}0\}_{Mg}$ (F2 and F3).

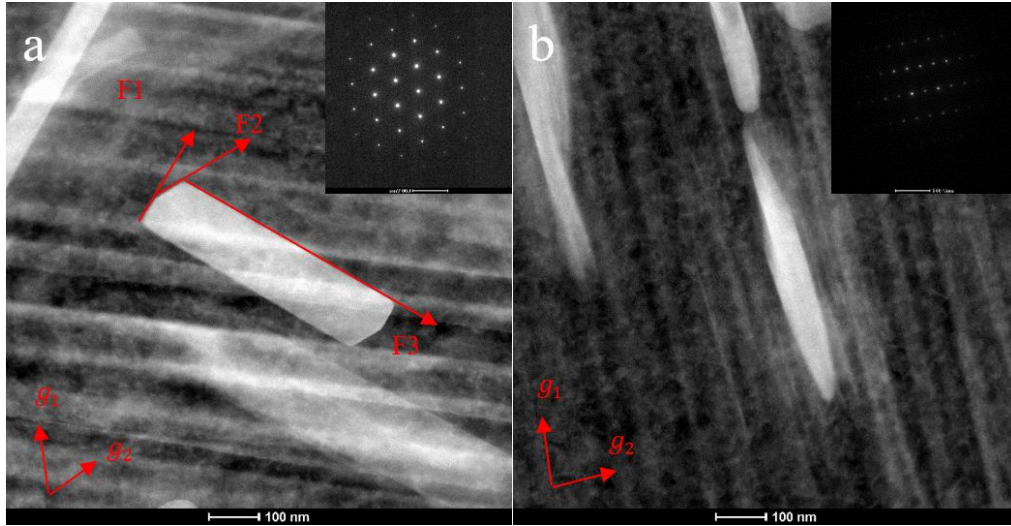


Figure 4 STEM-HAADF image showing the morphology of a Type 2 basal lath, (a) $B \approx [0001]_{Mg}$, $g_1 = 10\bar{1}0_{Mg}$, $g_2 = 01\bar{1}0_{Mg}$, (b) $B \approx [11\bar{2}0]_{Mg}$, $g_1 = 1\bar{1}00_{Mg}$, $g_2 = 0002_{Mg}$

A selected area diffraction pattern showing the OR between the Type 2 precipitates and the Mg- matrix can be found in Figure 5. As can be seen from the diffraction pattern, the OR between the Mg-matrix and the Type 2 precipitates is $(0001)_{Mg} \parallel (110)_{Mg2Sn}$, $[2\bar{1}\bar{1}0]_{Mg} \parallel [1\bar{1}1]_{Mg2Sn}$. This OR is equivalent to the OR2 first reported by Henes & Gerold and also reported in some other studies[3]–[5].

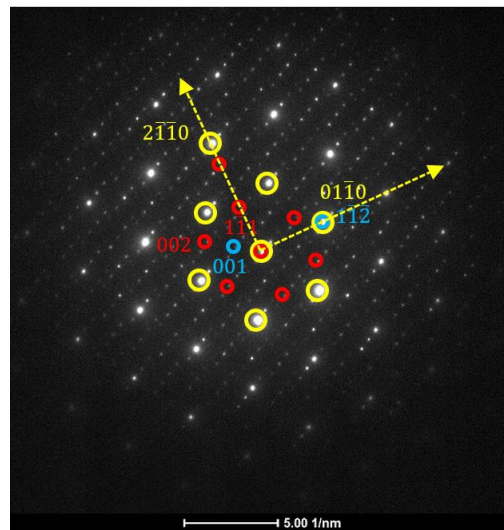


Figure 5 Selected area diffraction pattern defining the OR between the Type 2 precipitates and the Mg matrix. Reflections from the $[0001]_{Mg}$ zone axis are marked with yellow circles and reflections from the $[110]_{Mg2Sn}$ zone axis are marked with red circles. A few forbidden reflections from the $[110]_{Mg2Sn}$ zone axis are marked with blue circles. The OR given by the diffraction pattern is $(0001)_{Mg} \parallel (110)_{Mg2Sn}$, $[2\bar{1}\bar{1}0]_{Mg} \parallel [1\bar{1}1]_{Mg2Sn}$

Peak-aged Mg-6Sn-3Al alloy

Four types of Mg_2Sn precipitate were identified in the Mg-6Sn-3Al ternary alloy. STEM-

HAADF images showing the microstructure of the Mg-6Sn-3Al alloy are shown below in Figure 6, with a magnified image in Figure 7 showing the exact morphology of the precipitates. The addition of Al leads to there being only one type of basal lath in the alloy, which will be called Type 3, accompanied by additional basal plates, c-axis rods and pyramidal laths, labelled Type 4, Type 5 and Type 6 respectively.

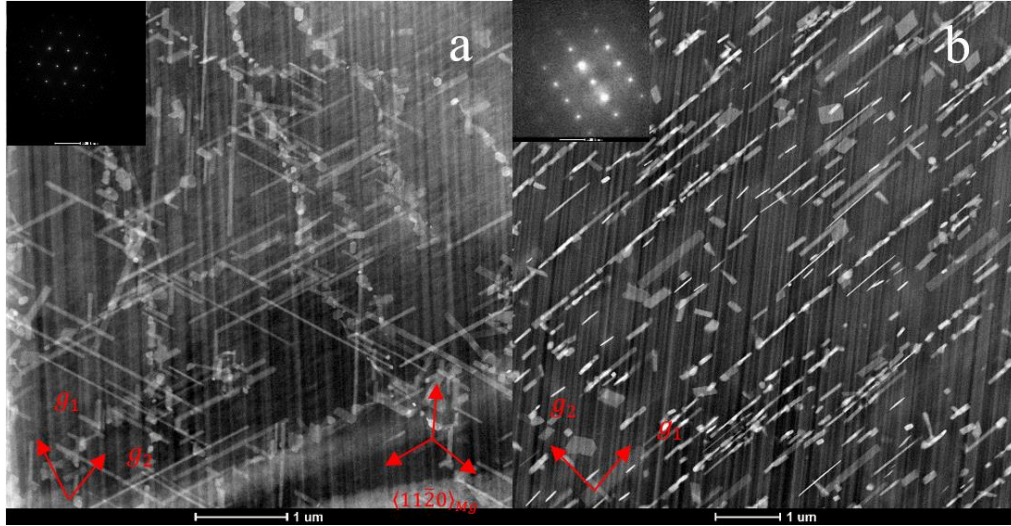


Figure 6 STEM-HAADF image showing the microstructure of the peak aged (72h) Mg-6Sn-3Al alloy, (a) $B \approx [0001]_{Mg}$, $g_1 = 10\bar{1}0_{Mg}$, $g_2 = 01\bar{1}0_{Mg}$, (b) $B \approx [1\bar{1}00]_{Mg}$, $g_1 = 11\bar{2}0_{Mg}$, $g_2 = 0002_{Mg}$

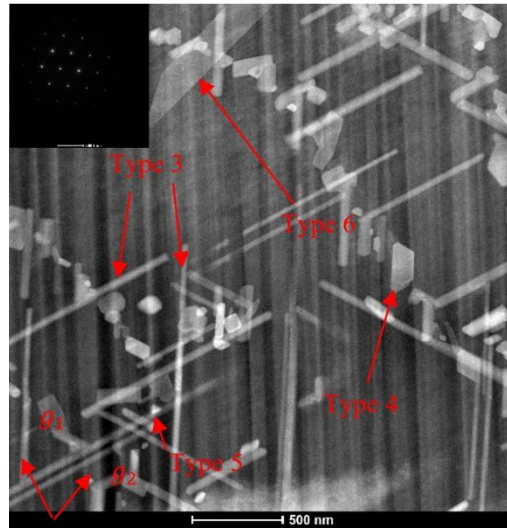


Figure 7 A higher magnification STEM-HAADF image of the peak aged Mg-6Sn-3Al alloy showing the different types of precipitates

Type 3 basal Mg_2Sn rods have their long axis parallel to the $\langle 11\bar{2}0 \rangle_{Mg}$ directions. A magnified image showing the exact morphology of a Type 3 precipitate can be found in Figure 8. Type 3 precipitates normally have a high aspect ratio, around 25:1. Some of the Type 3 precipitates have their tips slightly faceted (as marked in Figure 8(a)). $F1$ is parallel to $\{11\bar{2}0\}_{Mg}$

and F2 is parallel to $\{10\bar{1}0\}_{Mg}$). Most of them, however, tend to have round tips.

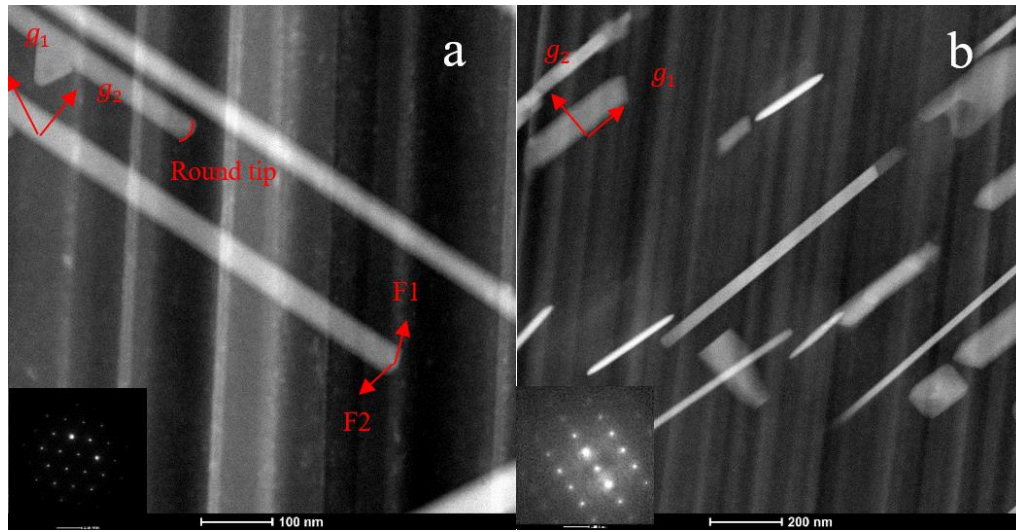


Figure 8 STEM-HAADF image showing the exact morphology of the Type 3 Mg_2Sn precipitates. (a) $B \approx [0001]_{Mg}$, $g_1 = 10\bar{1}0_{Mg}$, $g_2 = 01\bar{1}0_{Mg}$, (b) $B \approx [1\bar{1}00]_{Mg}$, $g_1 = 11\bar{2}0_{Mg}$, $g_2 = 0002_{Mg}$.

A selected area diffraction pattern showing the OR between the Type 3 precipitates and the Mg-matrix appears in Figure 9. Therefore, the OR between the Mg-matrix and the Type 3 precipitates can be determined as $(0001)_{Mg} \parallel (111)_{Mg_2Sn}$, $[11\bar{2}0]_{Mg} \parallel [1\bar{1}0]_{Mg_2Sn}$. First determined by Henes & Gerold as OR4, this OR is one of the most commonly reported ORs between the Mg matrix and a Mg_2Sn precipitate [2]–[4], [6]–[8].

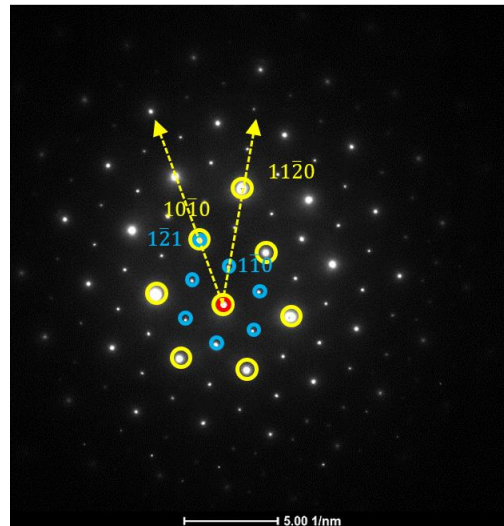


Figure 9 Selected area diffraction pattern defining the OR between the Type 3 precipitates and the Mg matrix. Reflections from the $[0001]_{Mg}$ zone axis are marked with yellow circles; forbidden reflections from the $[110]_{Mg_2Sn}$ zone axis are marked with blue circles. The OR defined by the diffraction pattern is $(0001)_{Mg} \parallel (111)_{Mg_2Sn}$, $[11\bar{2}0]_{Mg} \parallel [1\bar{1}0]_{Mg_2Sn}$.

The addition of Al also caused basal Mg_2Sn plates to appear in the alloy. These plate-shaped precipitates inhabit the basal plane and will be called Type 4 basal plates. The morphology of this type of precipitate is illustrated in Figure 10. Type 4 basal plates are obviously faceted with their 3 sets of facets parallel to $\{11\bar{2}0\}_{\text{Mg}}$, as marked in Figure 10.

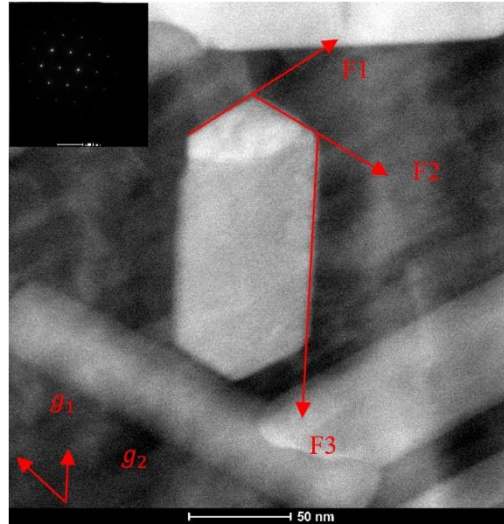


Figure 10 STEM-HAADF micrographs showing the morphology of the Type 4 basal plates, $B \approx [0001]_{\text{Mg}}$, $g_1 = 11\bar{2}0_{\text{Mg}}$, $g_2 = 1\bar{2}10_{\text{Mg}}$

A selected area diffraction pattern from a Type 4 basal plate is shown below in Figure 11. The diffraction pattern is identical to those from precipitate Type 3. The OR between the Type 4 precipitates and the Mg matrix is $(0001)_{\text{Mg}} \parallel (111)_{\text{Mg}_2\text{Sn}}$, $[11\bar{2}0]_{\text{Mg}} \parallel [1\bar{1}0]_{\text{Mg}_2\text{Sn}}$, namely OR4.

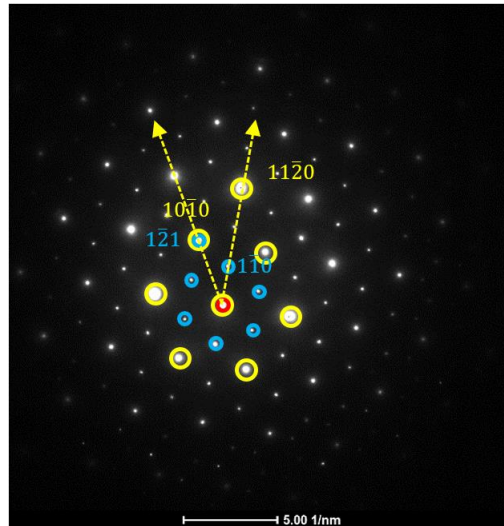


Figure 11 Selected area diffraction pattern from a Type 4 basal plate defining OR4. Reflections from the $[0001]_{\text{Mg}}$ zone axis are marked with yellow circles; forbidden reflections from the $[110]_{\text{Mg}_2\text{Sn}}$ zone axis are marked with blue circles. The OR given by the diffraction pattern is $(0001)_{\text{Mg}} \parallel (111)_{\text{Mg}_2\text{Sn}}$, $[11\bar{2}0]_{\text{Mg}} \parallel [1\bar{1}0]_{\text{Mg}_2\text{Sn}}$

One type of c-axis Mg_2Sn rod has also been found in the peak aged Mg-6Sn-3Al alloy. When observed from the $[0001]_{\text{Mg}}$ direction, these precipitates exhibit a triangular cross-section, with the three facets parallel to $\{11\bar{2}0\}_{\text{Mg}}$. The long axis is parallel to $[0001]_{\text{Mg}}$ when observed along $[10\bar{1}0]_{\text{Mg}}$. Therefore, this precipitate type is categorized as a Type 5 c-axis rod. A STEM-HAADF image showing its exact morphology appears in Figure 12.

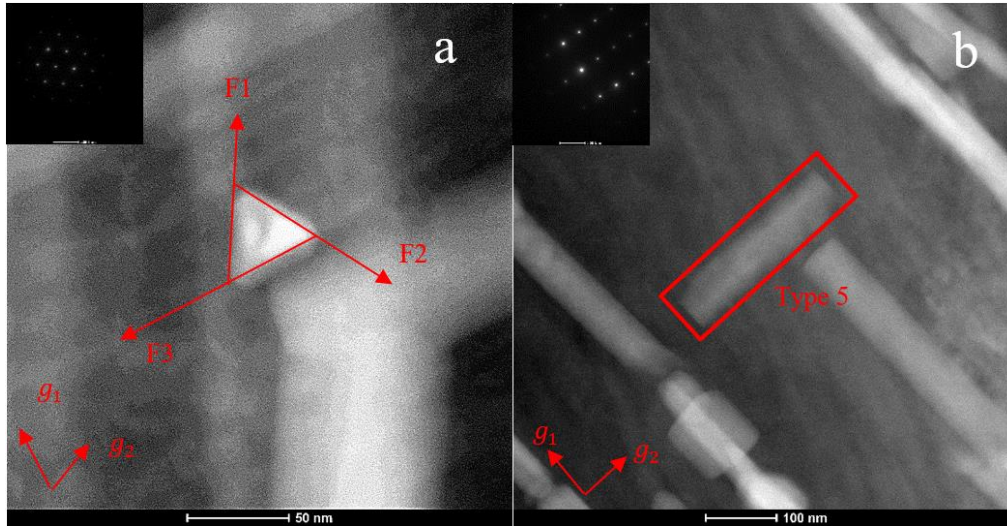


Figure 12 STEM-HAADF images showing the exact morphology of the Type 5 c-axis rods, (a) $B \approx [0001]_{\text{Mg}}$, $g_1 = 10\bar{1}0_{\text{Mg}}$, $g_2 = 01\bar{1}0_{\text{Mg}}$, (b) $B \approx [1\bar{1}00]_{\text{Mg}}$, $g_1 = 11\bar{2}0_{\text{Mg}}$, $g_2 = 0002_{\text{Mg}}$.

A selected area diffraction pattern acquired from the precipitate is shown below in Figure 13. The OR between the Type 5 c-axis rods and the Mg matrix is $(0001)_{\text{Mg}} \parallel (111)_{\text{Mg}_2\text{Sn}}$, $[11\bar{2}0]_{\text{Mg}} \parallel [1\bar{1}0]_{\text{Mg}_2\text{Sn}}$, i.e. OR4.

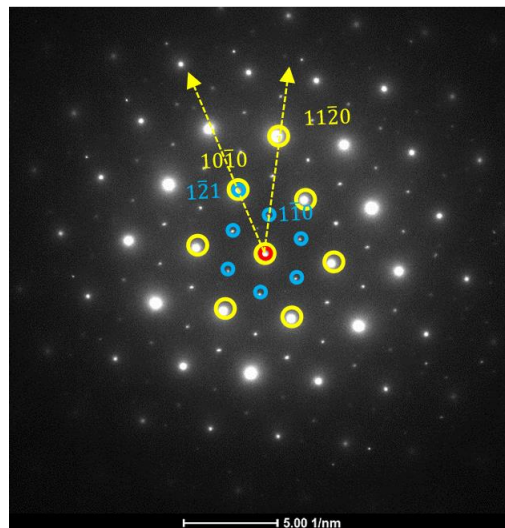


Figure 13 Selected area diffraction pattern demonstrating the OR between the Type 5 c-axis rods and the Mg matrix. Reflections from the $[0001]_{\text{Mg}}$ zone axis are marked with yellow circles; forbidden reflections from the $[110]_{\text{Mg}_2\text{Sn}}$ zone axis are marked with blue circles. The OR given by the diffraction pattern is $(0001)_{\text{Mg}} \parallel (111)_{\text{Mg}_2\text{Sn}}$, $[11\bar{2}0]_{\text{Mg}} \parallel [1\bar{1}0]_{\text{Mg}_2\text{Sn}}$

Pyramidal laths also were found in the Mg-6Sn-3Al alloy. These precipitates are categorised as Type 6 pyramidal laths. TEM tilting series confirmed that these precipitates have a first order pyramidal habit plane. An example of a tilting series for two pyramidal laths is shown below in Figure 14. An image was taken every 15° of α -tilt.

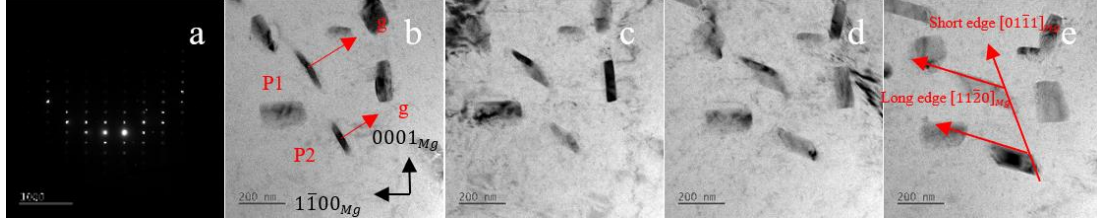


Figure 14 Tilting series for two pyramidal laths (a) Diffraction pattern showing the near- $[11\bar{2}0]_{Mg}$ beam direction at $\alpha \sim -15^\circ$ tilt (b) $\alpha \sim -15^\circ$, both precipitates are edge-on. $B \approx [11\bar{2}0]_{Mg}$ and the g -vector defining the habit plane is $11\bar{0}1_{Mg}$ (c) $\alpha \sim 0^\circ$, (d) $\alpha \sim 15^\circ$, (e) $\alpha \sim 30^\circ$; the long and short edges of the laths are marked in the figure.

Thus, these particular precipitates lie on $(1\bar{1}01)_{Mg}$. The OR for these pyramidal precipitates appears to be rather variable. For example, the diffraction patterns for P1 and P2 are shown below in Figure 15, where the reflections from Mg are marked yellow and those from Mg_2Sn are marked red. For P1, the orientation relationship with the Mg-matrix is $(11\bar{2}0)_{Mg} \parallel (110)_{Mg_2Sn}$, $[1\bar{1}01]_{Mg} \parallel [1\bar{1}3]_{Mg_2Sn}$ and that for P2 is $(11\bar{2}0)_{Mg} \parallel (110)_{Mg_2Sn}$, $[1\bar{1}01]_{Mg} \parallel [1\bar{1}5]_{Mg_2Sn}$. This variability, if it truly exists, is not currently understood.

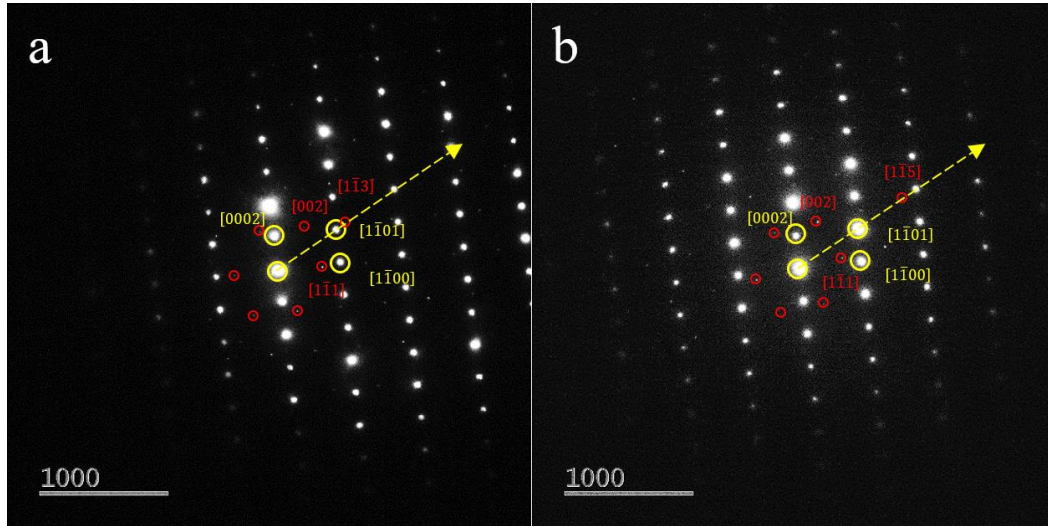


Figure 15 Diffraction patterns showing the OR between P1 (a), P2 (b) and the Mg-matrix. For P1, the OR given by the diffraction pattern is $(11\bar{2}0)_{Mg} \parallel (110)_{Mg_2Sn}$, $[1\bar{1}01]_{Mg} \parallel [1\bar{1}3]_{Mg_2Sn}$, for P2, the OR given by the diffraction pattern is $(11\bar{2}0)_{Mg} \parallel (110)_{Mg_2Sn}$, $[1\bar{1}01]_{Mg} \parallel [1\bar{1}5]_{Mg_2Sn}$.

Some previous research also reported the habit planes of pyramidal Mg_2Sn precipitates in Mg alloys. Sasaki *et al.* reported pyramidal laths with $\{11\bar{2}2\}_{Mg}$ habit planes and $\langle 10\bar{1}0 \rangle_{Mg}$ long axes,

but without specifying the orientation relationship[9]. No other research either confirms or denies this.

Peak-aged Mg-6Sn-3Zn alloy

The morphology and crystallography of the precipitates in the ternary Mg-6Sn-3Zn alloy are different from those in the other two alloys. Except for the presence of Type 2 basal laths, prismatic Mg_2Sn laths (Type 7) and c-axis MgZn_2 rods are also found in the alloy. In addition, most of the MgZn_2 rods and Type 2 basal laths are connected, forming a T-shaped morphology. A STEM-HAADF image showing the general microstructure of the peak aged Mg-6Sn-3Zn alloy appears in Figure 16, with all the precipitate types marked.

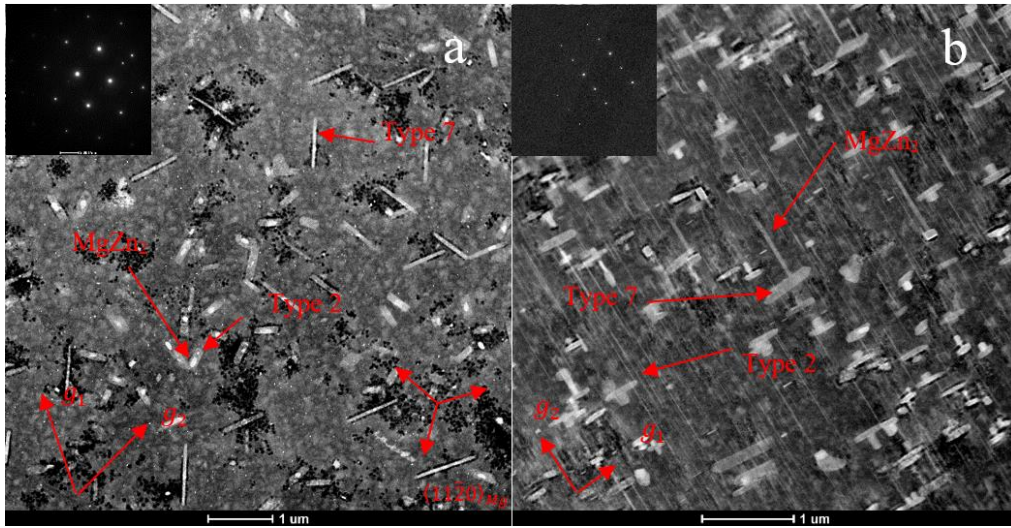


Figure 16 STEM-HAADF images showing the general microstructure of the precipitates in the peak aged Mg-6Sn-3Zn alloy, (a) $B \approx [0001]_{Mg}$, $g_1 = 10\bar{1}0_{Mg}$, $g_2 = 01\bar{1}0_{Mg}$, (b) $B \approx [1\bar{1}00]_{Mg}$, $g_1 = 11\bar{2}0_{Mg}$, $g_2 = 0002_{Mg}$.

The Type 2 basal Mg_2Sn laths observed in the Mg-6Sn-3Zn alloy are slightly different from those in the binary Mg-6Sn alloy. Similarly to the Type 2 basal laths found in the binary Mg-6Sn alloy, they have their long axis parallel to the $\langle 10\bar{1}0 \rangle_{Mg}$ directions and 3 facets parallel to $\{10\bar{1}0\}_{Mg}$. The difference is that most of the Type 2 basal laths are connected to a prismatic MgZn_2 rod, which is a commonly reported phenomenon in the Mg-Sn-Zn alloys and is enlarged upon in the discussion in the main paper. STEM-HAADF images showing the exact morphology of the Type 2 basal lath are shown below in Figure 17, along with a magnified image (from Figure 17(a)) in Figure 18 marking all the facets of a Type 2 precipitate.

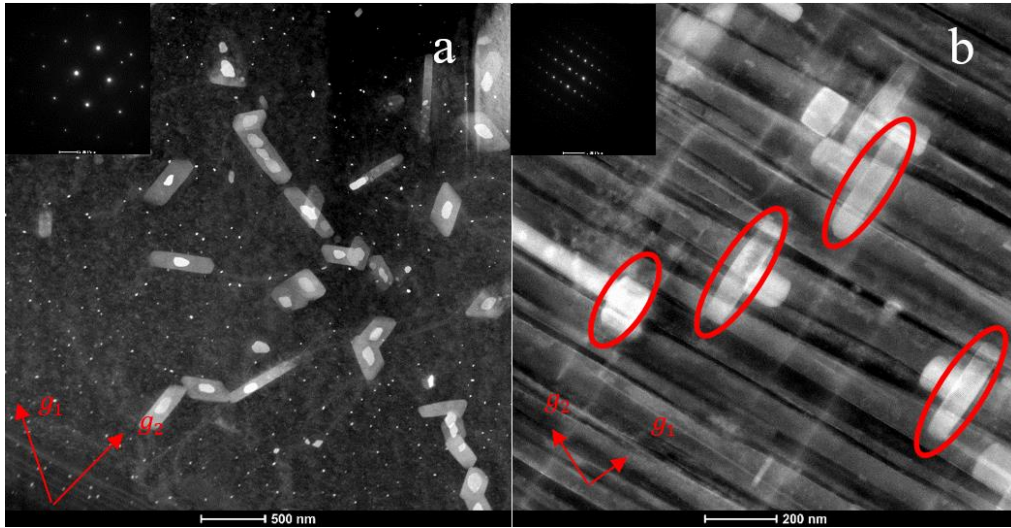


Figure 17 STEM-HAADF images showing the morphology of the Type 2 basal laths in the Mg-6Sn-3Zn ternary alloy. (a) $B \approx [0001]_{Mg}$, $g_1 = 10\bar{1}0_{Mg}$, $g_2 = 01\bar{1}0_{Mg}$, (b) $B \approx [11\bar{2}0]_{Mg}$, $g_1 = 1\bar{1}00_{Mg}$, $g_2 = 0002_{Mg}$. Type 2 laths are marked with circles. The small bright dots in (a) are the narrow $MgZn_2$ laths.

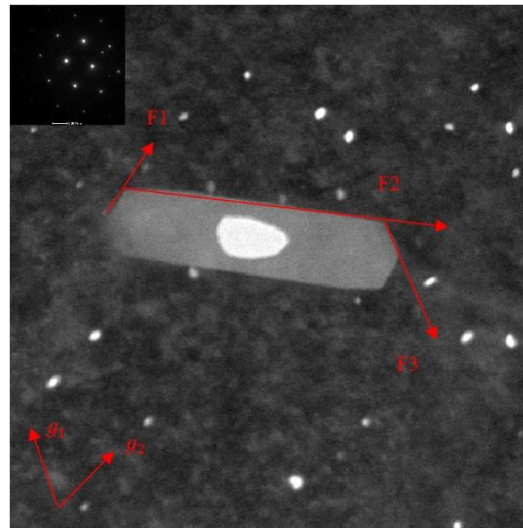


Figure 18 Magnified image of a Type 2 basal lath showing its three $\{10\bar{1}0\}_{Mg}$ facets. $B \approx [0001]_{Mg}$, $g_1 = 10\bar{1}0_{Mg}$, $g_2 = 01\bar{1}0_{Mg}$

The Type 2 basal laths in the ternary Mg-6Sn-3Zn alloy exhibit the same OR as those in the binary alloy. A selected area diffraction pattern showing this appears in Figure 19. The OR between the Mg-matrix and the Type 2 basal laths in the Mg-6Sn-3Zn ternary alloy can be determined as $(0001)_{Mg} \parallel (110)_{Mg2Sn}$, $[2\bar{1}\bar{1}0]_{Mg} \parallel [1\bar{1}1]_{Mg2Sn}$, namely OR2.

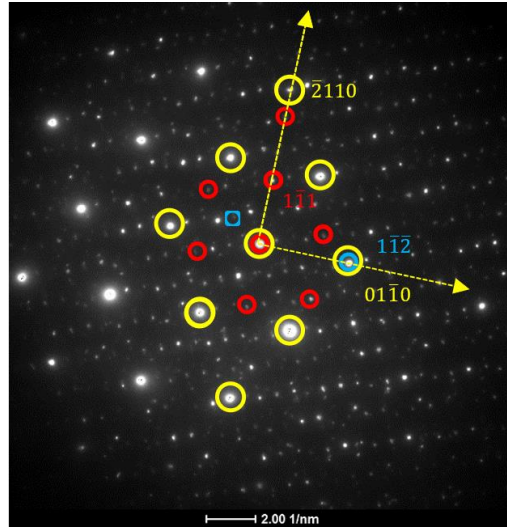


Figure 19 Selected area diffraction pattern showing the OR between the Type 2 basal laths and the Mg-matrix. The OR defined by the diffraction pattern is $(0001)_{Mg} \parallel (110)_{Mg_2Sn}$, $[2\bar{1}\bar{1}0]_{Mg} \parallel [\bar{1}\bar{1}1]_{Mg_2Sn}$.

The addition of Zn to the binary Mg-6Sn alloy resulted in a new type of prismatic Mg_2Sn lath with its long axis parallel to the three $\langle 11\bar{2}0 \rangle_{Mg}$ directions. These precipitates are obviously narrower than the Type 2 basal laths and have an aspect ratio of $\sim 8:1$. They have relatively larger dimensions on the prismatic $\{11\bar{2}0\}_{Mg}$ planes than on the basal. Therefore, these precipitates are categorized as Type 7 prismatic laths. STEM-HAADF images showing the morphology of the Type 7 prismatic laths can be found below in Figure 20, with the Type 7 prismatic laths marked with circles. Another image with the Type 7 prismatic lath edge-on is shown in Figure 21.

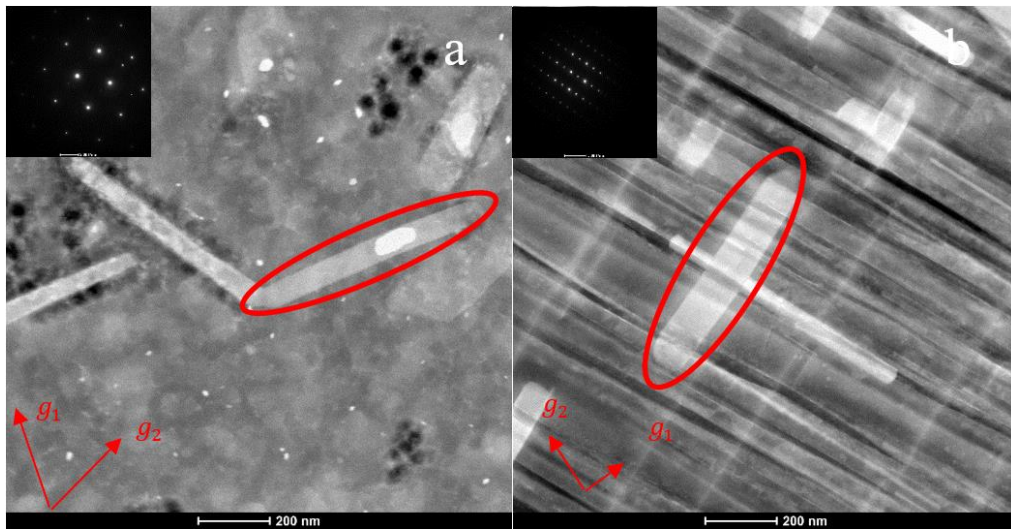


Figure 20 STEM-HAADF images showing the morphology of the Type 7 prismatic laths, (a) $B \approx [0001]_{Mg}$, $g_1 = 10\bar{1}0_{Mg}$, $g_2 = 01\bar{1}0_{Mg}$, (b) $B \approx [11\bar{2}0]_{Mg}$, $g_1 = 1\bar{1}00_{Mg}$, $g_2 = 0002_{Mg}$.

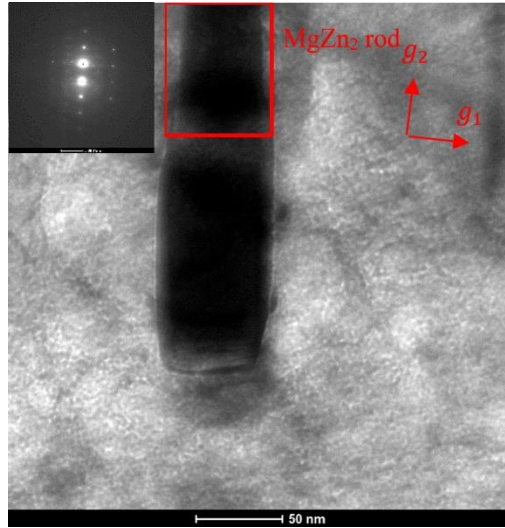


Figure 21 STEM-BF image showing a Type 7 prismatic lath edge-on. $B \approx [11\bar{2}0]_{Mg}$, $g_1 = 1\bar{1}00_{Mg}$, $g_2 = 0002_{Mg}$. A c-axis $MgZn_2$ rod is marked with a rectangle, the precipitate below the rectangle is the Type 7 lath.

For the selected area diffraction patterns shown below in Figure 22, the diffraction patterns from the Mg-matrix and the precipitate can be indexed as $[0001]_{Mg}$ and $[110]_{Mg2Sn}$ respectively with the OR being $(0001)_{Mg} \parallel (110)_{Mg2Sn}$, $[11\bar{2}0]_{Mg} \parallel [001]_{Mg2Sn}$, which is OR1. The diffraction patterns taken from the Type 7 prismatic laths are therefore similar to those from the Type 1 basal laths. Shi and Zhang observed similar precipitation behaviour in a Mg-Sn-Zn-Mn alloy although the precipitate they reported is not perfectly parallel to the basal plane and the OR is also 0.39° deviated from OR1 and is named “near OR1” [10]. The precipitates reported in this work are exactly parallel to the basal plane and have the precise OR1 relationship.

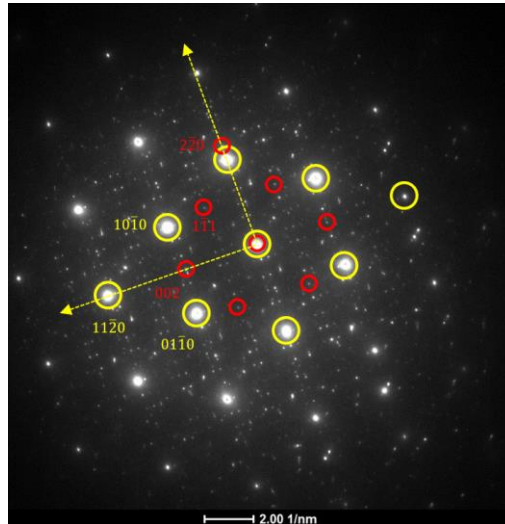


Figure 22 Selected area diffraction pattern indicating the OR between the Type 7 prismatic laths and the Mg-matrix. The OR given by the diffraction pattern is $(0001)_{Mg} \parallel (110)_{Mg2Sn}$, $[11\bar{2}0]_{Mg} \parallel [001]_{Mg2Sn}$.

Differently from the Al which is homogeneously distributed in the Mg-6Sn-3Al ternary alloy, Zn tends to form its own MgZn_2 precipitates in the Mg-6Sn-3Zn alloy. This phase has a HCP structure with the space group $P6_3/mmc$ ($a=0.525\text{nm}$, $c=0.845\text{nm}$). There are two distinguishable types of MgZn_2 precipitate in the alloy: prismatic MgZn_2 wide rods and prismatic MgZn_2 narrow rods. STEM-HAADF images showing the morphology of the MgZn_2 precipitates are shown below in Figure 23. As can be seen from the images, the precipitates with long axis parallel to the $[0001]_{\text{Mg}}$ direction are brighter than the attached Mg_2Sn precipitates, which suggests a higher average atomic mass. These prismatic precipitates are the MgZn_2 rods.

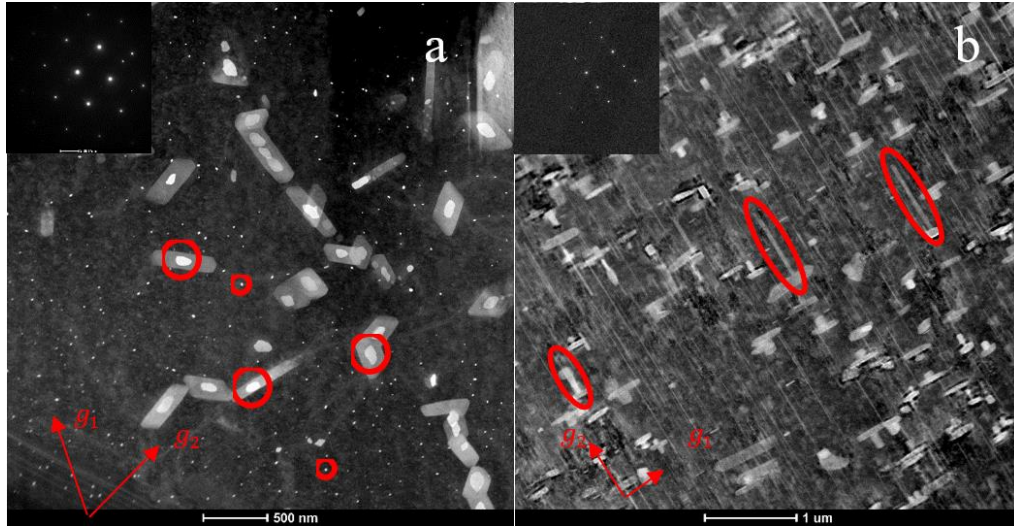


Figure 23 STEM-HAADF images showing the morphology of the MgZn_2 precipitates, (a) $B \approx [0001]_{\text{Mg}}$, $g_1 = 10\bar{1}0_{\text{Mg}}$, $g_2 = 01\bar{1}0_{\text{Mg}}$, (b) $B \approx [11\bar{2}0]_{\text{Mg}}$, $g_1 = 1\bar{1}00_{\text{Mg}}$, $g_2 = 0002_{\text{Mg}}$. The small circles mark the narrow MgZn_2 rods.

A diffraction pattern showing the OR between the MgZn_2 precipitates and the matrix can be found below in Figure 24, with the reflections from the Mg-matrix marked in yellow and those from the MgZn_2 precipitate marked in red. The diffraction pattern from the Mg-matrix can be indexed as $[11\bar{2}0]_{\text{Mg}}$ while that from the MgZn_2 precipitates can be indexed as $[10\bar{1}0]_{\text{MgZn}_2}$. The OR between the Mg-matrix and the MgZn_2 precipitates can then be determined as $(0001)_{\text{Mg}} \parallel (11\bar{2}0)_{\text{MgZn}_2}$, $[11\bar{2}0]_{\text{Mg}} \parallel [10\bar{1}0]_{\text{MgZn}_2}$.

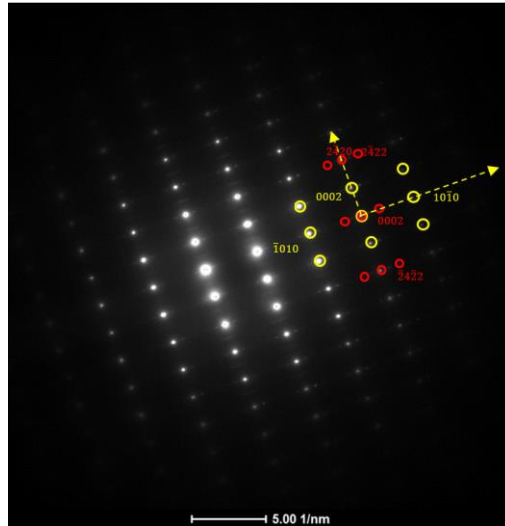


Figure 24 Selected area diffraction pattern showing the OR between the MgZn_2 precipitate and the Mg-matrix. The OR given by the diffraction pattern is $[0001]_{\text{Mg}} \parallel [11\bar{2}0]_{\text{MgZn}_2}$, $[10\bar{1}0]_{\text{Mg}} \parallel [0001]_{\text{MgZn}_2}$, $[11\bar{2}0]_{\text{Mg}} \parallel [10\bar{1}0]_{\text{MgZn}_2}$.

References:

- [1] T. T. Sasaki, J. D. Ju, K. Hono, and K. S. Shin, "Heat-treatable Mg-Sn-Zn wrought alloy," *Scr. Mater.*, vol. 61, no. 1, pp. 80–83, 2009, doi: 10.1016/j.scriptamat.2009.03.014.
- [2] M. Zhang, W. zheng Zhang, G. zhen Zhu, and K. Yu, "Crystallography of Mg₂Sn precipitates in Mg-Sn-Mn-Si alloy," *Trans. Nonferrous Met. Soc. China (English Ed.)*, vol. 17, no. 6, pp. 1428–1432, 2007, doi: 10.1016/S1003-6326(07)60289-1.
- [3] S. Henes and V. Gerold, "Röntgenographische Untersuchungen der Ausscheidungsvorgänge in Magnesium-Blei- und Magnesium-Zinn-Legierungen," *Zeitschrift für Met.*, vol. 53, p. 743, 1962.
- [4] T. T. Sasaki, K. Oh-ishi, T. Ohkubo, and K. Hono, "Enhanced age hardening response by the addition of Zn in Mg–Sn alloys," *Scr. Mater.*, vol. 55, no. 3, pp. 251–254, 2006, doi: 10.1016/j.scriptamat.2006.04.005.
- [5] X. Zhang, M. Wang, R. He, W. Li, and B. Y. Zong, "A phase field model to simulate competitive precipitation of Mg₂Sn along the basal or pyramidal habit planes in Mg-2.2Sn-0.1Zn alloy," *Comput. Mater. Sci.*, vol. 127, pp. 261–269, 2017, doi: 10.1016/j.commatsci.2016.10.019.
- [6] C. L. Mendis, C. J. Bettles, M. A. Gibson, S. Gorsse, and C. R. Hutchinson, "Refinement of precipitate distributions in an age-hardenable Mg-Sn alloy through microalloying," *Philos. Mag. Lett.*, vol. 86, no. 7, pp. 443–456, 2006, doi: 10.1080/09500830600871186.
- [7] C. L. Mendis, C. J. Bettles, M. A. Gibson, and C. R. Hutchinson, "An enhanced age hardening response in Mg-Sn based alloys containing Zn," *Mater. Sci. Eng. A*, vol. 435–436, pp. 163–171, 2006, doi: 10.1016/j.msea.2006.07.090.
- [8] F. R. Elsayed, T. T. Sasaki, C. L. Mendis, T. Ohkubo, and K. Hono, "Compositional optimization of Mg-Sn-Al alloys for higher age hardening response," *Mater. Sci. Eng. A*, vol. 566, pp. 22–29, 2013, doi: 10.1016/j.msea.2012.12.041.
- [9] T. T. Sasaki, K. Oh-ishi, T. Ohkubo, and K. Hono, "Effect of double aging and microalloying on the age hardening behavior of a Mg-Sn-Zn alloy," *Mater. Sci. Eng. A*, vol. 530, no. 1, pp. 1–8, 2011, doi: 10.1016/j.msea.2010.05.010.
- [10] Z. Z. Shi and W. Z. Zhang, "Newly observed prismatic Mg₂Sn laths in a Mg-Sn-Zn-Mn alloy," *J. Mater. Sci.*, vol. 48, no. 21, pp. 7551–7556, 2013, doi: 10.1007/s10853-013-7570-8.